substance: boron compounds with lanthanides
property: properties of lanthanide hexaborides: EuB_6

Structure, chemical bond

Growth and crystal data for preparation by high temperature solution growth [84L] and references therein.

On the pressureless sintering of europium-hexaboride [87K].

Homogeneity range: $Eu_{0.9}B_6$ ... $EuB_{5.93}$ (see [98S] and references therein)

Structural anomaly in the the range of magnetic transitions [98S].

lattice parameters

a	4.1780 Å	*T* = 300 K	see also [56P] and [74M1]	73S, 77E, 79G
	4.186 Å		see Fig. 1, see also [74M1]	78K, 79K
	4.1849(1) Å		single crystal X-ray diffraction	95B

lattice parameters in the homogeneity range

a	4.1844(5)	*T* = 304 K	EuB_6, X-ray diffraction,	83P
	4.1849(2)		$Eu_{0.79}B_6$	

interatomic distances
(in Å)

d	1.7596(12)	B – B	95B
	1.6954(17)	B – B’	
	3.0783(3)	B – Me	

Electronic properties

EuB_6 is a magnetic semiconductor. It has been assumed that the Eu^{2+}:$4f^7$ level is located in the band gap. Eu vacancies would introduce holes in the $4f^7$ configuration. These holes are small polarons, i.e. Eu^{3+} ions trapped by electrostatic forces on a site near-neighbor to the vacancy (acceptor density n_a) The negative Seebeck coefficient indicates that electron donor sites with $n_d > n_a$ are also present. These are rare earth atoms as substitutional impurities, represented in Fig. 2 by $5D^1$ donor levels of Ln^{2+}:$4f^{n-l}5d^1$ centers. When the density of the impurity atoms is sufficient, a narrow, partly occupied $5d^1$ impurity band is formed [77E, 73G]. Some experimental results seem not to agree satisfactorily with this band scheme [77I, 79F, 79W].

The semiconducting behavior in the paramagnetic region changes to semimetallic behavior at the ferromagnetic ordering temperature T_C = 13.7 K [81T; 80G1].

Self-consistent APW calculation of the electronic energy band structure in Fig. 3 [80H1].

Calculated density of states in the vicinity of the Fermi level in Fig. 4 [80H1].

energy gap

E_g	~1 eV	*T* = 300 K	derived from optical absorption	80G2
	43 meV	*T* = 7.2...46 K	electron-tunneling	98A

An energy diagram for EuB_6 is shown in Fig. 2; for band structure calculation, cf. [75P, 77P].

energy gaps (or activation energies for conduction)

E_g	0.38 eV		electrical conductivity	69F
	0.30 eV		electrical conductivity	73G, 77E
	0.032 eV		electrical conductivity (cp. remark below (impurity and defects))	80L
	0.05...0.1 eV		electrical conductivity	81T

pressure dependence of the energy gap

dE_g/dp	– 1.5meV/kbar	T = 300K		80L

optical transition energies
(in meV):

high-purity EuB_6:

E_g	9.55(10)	300 K	impurity to band	99W
	13.2(3)		impurity to band or direct forbidden interband	
	20.1(5)		direct allowed interband	
	32.8(2)			

carbon-doped EuB_6 (1.1 at. % C total; 0.81 at. % C substituted for B atoms in the structure):

E_g	7.6(3)	T = 300 K	impurity to band	99W
	15(1)		impurity to band or direct forbidden interband	
	34(3)		direct allowed interband	
δE_C	18	T = 300K	carbon donor level (estimated from carrier concentration depending on C content)	99W

FIR absorption spectrum in Fig. 5 [99W].

***g*-factors**

g	2.004(1)	ESR	72H
	2.000(2)	ESR	76G1, 76G2
	1.995(10)	ESR	79O

For temperature dependence of ESR resonance points and linewidth, see Fig. 6; for further ESR investigations, see [73S1, 73S2, 75G1, 75G2, 76G2, 76G3, 76G4, 79M1, 79K1].

effective mass of electrons

m_n	0.225 m_0	T = 300 K		99A

Optical absorption spectrum in the range of the absorption edge in Fig. 7 [80G2].

reflectivity maxima indicating high energy interband transitions
(E in eV)

$E(R_{max})$	3.5	T = 300 K	reflectivity spectra	90G
	5.5			
	7.1			
	9.4			
	11.6			
	15			

FIR absorption spectrum in Fig. 5 [99W].

average inner lattice potential

Φ	12.7 eV	experiment	86K
	11.03 eV	theory	

average work function of electrons

Φ_e	4.11 eV	experiment	86K
	5.778 eV	theory	

B K emission and absorption spectrum (compared with SmB_6 and LaB_6) in [82O].

Impurities and defects

The electronic properties of EuB_6 are strongly influenced by carbon. Even very small C contents (C substitutional on B sites) lead to a degenerate semiconductor, in which carrier concentration and antiferromagnetic interaction increase with C content [81T]. Possibly many of the experimental results available are influenced in this way.

For effects of carbon on lattice parameter, paramagnetic Curie temperature and resistivity, see Figs. 1, 8, 9; for effects on the magnetism of EuB_6, see [79K].

$EuB_{6-x}C_x$

In [81T1] the carbon atoms are assumed to be associated in pairs in the covalent B-C sublattice. Each carbon pair introduces two extra electrons in the material, one being localized in the anionic sublattice and the other delocalized in the conduction band. This assumption is in contrast to [99W], where the results seem to indicate that the C atoms are statistically distributed on single regular B sites and act as donors with activation energies, that are similar to those in classical semiconductors.

On the pressureless sintering of europium-hexaboride [87K].

lattice parameters

a	4.1835(5) Å	*T* = 300 K	x = 0.03, X-ray diffraction	81T
	4.1818(5) Å		x = 0.05	

Variation of the lattice parameters depending on the C content and indicating the solubility limits for different temperatures in Fig. 10 [78K].

Variation of the carrier concentration depending on the C content in Fig. 11 [99W].

ESR study of $EuB_{6-x}C_x$ including the comparison with some corresponding $YbB_{6-x}C_x$, $SrB_{6-x}C_x$, $Eu_{1-x}Gd_xB_6$, $Eu_{1-x}Sr_xB_6$ and $Eu_{1-x}La_xB_6$ compounds in [81T].

Paramagnetic Curie temperature depending on carbon content in Fig. 12 [81T].

carrier concentration

deduced from Hall effect using a one-band model (in cm^{-3})

n_e	$1.74 \cdot 10^{20}$	$EuB_{5.97}C_{0.03}$	81T
	$2.3(5) \cdot 10^{20}$	$EuB_{5.95}C_{0.05}$	

plasma frequencies and derived carrier concentrations (T = 300 K)

ν_p [s^{-1}]	n_e [cm^{-3}]		
$2.4 \cdot 10^{14}$	$2.5 \cdot 10^{19}$	high-purity (C< 0.1 at. %)	99W
$9.1 \cdot 10^{14}$	$4.1 \cdot 10^{20}$	C = 1.1 at. % total; 0.81 at. % substituted for B	
$2.4 \cdot 10^{14}$	$7.8 \cdot 10^{20}$	C = 1.43 at.%	

Lattice properties

phonon wavenumbers of $EuB_{5.9}C_{0.1}$
(in cm^{-1})

ν/c	1247 1185 1110 776 271 258 167 122	T = 300 K	FT Raman	97S

FT-Raman spectrum of $EuB_{5.9}C_{0.1}$ in Fig. 13 [97S].

Raman spectrum and frequencies see also **properties of lanthanide hexaborides: YbB_6** (Optical prop.)

IR phonon wavenumbers

ν/c	860 cm^{-1} 147 cm^{-1}	T = 300 K		99W

IR reflectivity spectrum in Fig. 14 [99W].

Transport properties

Pressure dependence of the electrical resistivity; $\rho(p)/\rho(0)$ vs. hydrostatic pressure p (compared with LaB_6, SmB_6 and YbB_6) in Fig. 15 [81K, 91S].

resistivity

ρ	$6.16 \cdot 10^{-4}$ Ω cm	T = 300 K	see Figs. 16, 17	80G1
	$8.47 \cdot 10^{-5}$ Ω cm	T = 300 K		75S
	$1 \cdot 10^{-2}$ Ω cm	T = 300 K	see Fig. 18	77E, 74M1
	2 Ω cm	T = 300 K	possibly carbon-doped	69P, 75S
	$5 \cdot 10^{-4}$ Ω cm	T = 300 K	semimetal	79F

pressure dependence of resistivity

$(d \log \rho/dp)_{p=0}$	$-27 \cdot 10^{-3}$ $kbar^{-1}$	T = 300 K	80L

For pressure dependence of resistivity (samples of different composition), see Fig. 19.

temperature coefficient of resistivity

$(1/\rho)d\rho/dT$	$+ 0.09 \cdot 10^{-2}$ K^{-1}	T = 300K	75S

resistivity ratios ρ(T)/ρ(300K) for $T = T_{c1}$ and T_{c2}
(T_{c1} and T_{c2}: ferromagnetic transition temperatures)

$\rho(T)/\rho(300K)$	T_{c1} [K]	T_{c2} [K]	
86	15.3	12.7	98S
35	14	9	80K
60	13.7	not observed	79F
52.5	13.7	not observed	80G1
1	(T_N ~ 5K)*)	not observed	77I
56	14.5	not observed	80W
40	12.5	not observed	78K

*) Antiferromagnetic transitions, induced by carbon impurities

Temperature dependence of the electrical resistivity between 1.5 and 300 K in Fig. 20 [98S].

Magnetoresistance measured for B || [100] at 15 K in Fig. 21 [98S].

electron concentration

n	$1.7 \cdot 10^{20}$ cm^{-3}	T = 4.2 K	electrical conductivity and Hall	80G1
	$3.5 \cdot 10^{19}$ cm^{-3}	T = 100...150 K	effect, see Fig. 22	
	$3 \cdot 10^{19}$ cm^{-3}	T = 4.2...300 K		79W

electron mobility

μ_n	2560 cm^2/V s	T = 4.2 K	electrical conductivity and	80G1
	300 cm^2/V s	T = 100...150 K	Hall effect	
	2000 cm^2/V s	T = 4.2 K		79W
	325 cm^2/V s	T = 77 K		
	100 cm^2/V s	T = 290 K		

pressure dependence of galvanometric effects

d log μ_n/dp	$10(4) \cdot 10^{-6}$ bar^{-1}	T = 4.2 K	79W
	$25(15) \cdot 10^{-6}$ bar^{-1}	T = 77 K	
	≈ 0	T = 290 K	

For pressure dependence of ρ, see Fig. 23, of magnetoresistance, see Fig. 24

For electrical conductivity, Hall effect of EuB_6, see also [73G, 73M, 76M, 77E, 81K]; for conductivity, carrier concentration, mobility of EuB_6 with deviations from exact stoichiometry, see [79G, 79C].

thermoelectric power

S	– 75 µV K^{-1}	T = 300 K	see Fig. 25 see also [73M]	73G
	– 17.7 µV K^{-1}	T = 300 K		75S
	– 38.5 µV K^{-1}	T = 300 K		69P

Pressure dependence of the thermoelectric power in Fig. 26 [81K, 91S].

For Hall coefficient, see [62S].

thermal conductivity

κ	19.26 W m^{-1} K^{-1}	T = 90°C	73S
	19 W m^{-1} K^{-1}	T = 90°C	81S

Optical properties

lattice dielectric constant
(derived by extrapolating ε_r in the range of the plasma edge, see Fig. 27)

ε_L	6.1(1)	T = 300 K	single crystal, high-purity (C< 0.1 at. %)	99W
	7.0(1)		C = 1.1 at. % total; 0.81 at. % substituted for B	
	8.9(1)		C = 1.43 at.%	

Dielectric function up to 42 eV in Fig. 28 [81S].

Reflectivity spectrum in Fig. 29 [81S].

For reflectivity see also [74M1, 74M2], see also **properties of lanthanide hexaborides: YbB_6** (Optical prop.).

IR reflectivity spectrum in Fig. 30 [99W].

Further properties

compressibility
(in Pa^{-1})

κ	$0.83 \cdot 10^{-11}$			80G1
	$0.60(3) \cdot 10^{-11}$	T = 300 K	pure EuB_6, X-ray power diffraction	82L
	$0.63 \cdot 10^{-11}$		$EuB_{6-x}C_x$, x ≈ 0.2	

heat capacity

see Fig. 31

density

d	4.938 g cm^{-3}	T = 300 K	X-ray	75S
	4.94 g cm^{-3}		pycnometric	73S
	4.91 g cm^{-3}		pycnometric	81S

melting point

T_m	2150°C			75S
	2580°C			73S
	> 2500°C			80H1
	≥ 2580 °C		melting with decomposition	96G

linear thermal expansion coefficient

α	$6.86 \cdot 10^{-6}$ K^{-1}	T = 300 K		75S
	$7.4 \cdot 10^{-6}$ K^{-1}	T = 293...1273 K		73S

work function

Φ	4.9 eV			75S
	3.95...403 eV	A = 29...120 A cm^{-2} K^{-2}	A is defined by $i_s = AT^2\exp(-\Phi/kT)$, where i_s is the saturation current density	78B
	4.32(7) eV			80F

emissivity at 655 mn

ε	0.83			75S

microhardness

H_K	1840 kg mm^{-2}	T = 300 K	Knoop hardness; load 1 N (see also [79F])	81S
	2140 kg mm^{-2}	T = 300 K	cube, average value; load 50 g	96G
	1780 kg mm^{-2}		cube, average value; load 200 g	

magnetic moment

p_{eff}	8.1 μ_B		effective magnetic moment	67P
	7.90(1) μ_B			79V
	7.76 μ_B			78F
p_{calc}	7.94 μ_B		theoretical (divalent Eu ion)	79V

ferromagnetic Curie temperature

T_C	8.5 K		polycrystal (?)	77B

	13.7 K	$Eu_{1-x}B_6$, single crystal	78F
	14 K	single crystal	79V
		polycrystal	77I, 68G

asymptotic (paramagnetic) Curie temperature

Θ_a	+ 9 K		77B, 67P

Entropy for ferromagnetic and antiferromagnetic EuB_6 in Fig. 32 [80F].

Field dependence of the specific heat between 0 and 10 T in Fig. 33 [98S].

Temperature dependence of the magnetic susceptibility in Fig. 34 [98S].

Temperature dependence of the exchange field (EuB_6): Fig.35; magnetic phase diagram ($Eu_{1-x}B_6$): Fig. 36.

For further investigations on ferromagnetism in EuB_6, see [71F, 71W, 73K, 74S, 75G1, 75G2, 76G1, 76G2, 76L, 77B2, 79V1].

Low field magnetic susceptibility of $Eu_{1-x}B_6$: Fig. 37 [79F].

References:

56P Post, B., Moskowitz, D., Glaser, F. W.: J. Am. Chem. Soc. 78 (1956) 1800.

62S Samsonov, G.V., Paderno, Yu.B.: in: Vsokotemperaturnaye metallokeramicheskie materialne, AN USSR: Kiev, 1962, p. 102 (in Russian).

67P Paderno, Yu.B., Pokrzywnicki, S.: Phys. Status Solidi 24 (1967) K11.

68G Geballe, T. H., Matthias, B. H., Andres, K., Maita, I. P., Copper, A. S., Corenzwit, E.: Science 160 (1968) 1443.

69F Fisk, Z., Matthias, B.T., Corenzwit, E.: Proc. Nat. Acad. Sci. 64 (1969) 1151.

69P Paderno, Yu.B., Novikov, V.I., Garf, E.S.: Poroshk. Metall. 11 (1969) 70 (in Russian).

70C Cooper, A.S., Corenzwit, E., Longinott, L.D., Matthias, B.T., Zachariasen, W.H.: Proc. Nat. Acad. Sci. 67 (1970) 313.

71F Fisk, Z.: Phys. Lett. 34 A (1971) 261.

71N Niihara, K.: Bull. Chem. Soc. Jpn. 44 (1971) 963.

71W Wood, V. E.: Phys. Lett. 37 A (1971) 357.

72H Hacker, H.: J. Magn. Reson. 8 (1972) 175.

73B Butcher, P.N., Morys, P.L.: J. Phys. C 6 (1973) 2147.

73G Gust, W.H., Holt, A.C., Roye, E.B.: J. Appl. Phys. 44 (1973) 550.

73K Krause, J. L., Sienko, M. J.: J. Solid State Chem. 6 (1973) 590.

73M Mott, N. F.: Philos. Mag. 30 (1973) 403.

73S Samsonov, G.V., Paderno, Yu.B., Levandovski, B.D., Konovalova, E.S.: in: Redkosemelnie metalli splabi i coedinenia, Isdatelstvo NAUKA ed., Moscow, 1973, p. 269 (in Russian).

73S1 Sperlich, G., Buschow, K. H. J.: Proc. 4th. Int. Conf Solid Comp. Trans. Elements, Geneva, 1973, p. 216.

73S2 Sperlich, G.: Int. J. Magn. 5 (1973) 125.

74M1 Mercurio, J.P., Etournoeau, J., Naslain, R., Hagenmuller, P., Goodenough, J.B: J. Solid State Chem. 9 (1974) 7.

74M2 Muranaka, S., Kawai, S.: J. Cryst. Growth 26 (1974) 165.

74S Sperlich, G., Jansen, K.: Solid State Commun. 15 (1974) 1105.

75G1 Glaunsinger, W. S.: Phys. Status Solidi (b) 70 (1975) K 151.

75G2 Glaunsinger, W. S.: J. Magn. Reson. 18 (1975) 265.

75P Paderno, Yu.B., Severianina, E.N., Dudnik, E.M., Lazorenko, V.I.: in: Refractory alloys of metals with special physica-chemical properties, Izdatel'stvo NAUKA ed., Moscow, 1975, p. 118 (in Russian).

75S Samsonov, G.V., Serebryakova, T.I., Neronov, V.A.: in: Boridy, Moskva Atomzidat, 1975.

76G1 Glaunsinger, W. S.: AIP Conf. Proc. 1976 (Magn. Mat. Ann. Conf. 21th, 1975) 412.

76G2 Glaunsinger, W. S.: Phys. Status Solidi (b) 74 (1976) 443.

76G3 Glaunsinger, W. S.: J. Phys. Chem. Solids 37 (1976) 51.

76G4 Glaunsinger, W. S.: J. Magn. Reson. 21 (1976) 147.

76L Lalanne, M., Georges, R., Mercuno, J. P., Chevalier, B., Etourneau, J.: J. Less-Common Met. 46 (1976) 39.

76M Matkovich, V. I.: J. Less-Common Met. 46 (1976) 39.

77B Becher, H.J., Mattes, R.: in Boron and Refractory Borides, V.I. Matkovich ed., Springer: Berlin, Heidelberg, New York, 1977, p. 107.

77B1 Berezin, A. A., Golikova, O. A., Zaitsev, V. R., Kazanin, M. M., Orlov, V. M., Tkalenko, E. N., in:Boron and Refractory Borides, (Matkovich V. 1., ed.) Springer: Berlin, Heidelberg, New York 1977, p. 52.

77B2 Buschow, K. H. J.: see [77B1], p. 494.

77E Etourneau, J., Mercurio, J.P., Hagenmuller, P.: in: Boron and Refractory Borides, V.I Matkovich ed., Springer: Berlin, Heidelberg, New York, 1977, p. 115.

77I Isikawa, Y., Bajaj, M.M., Kusaya, M., Tanaka, T, Bannay, E.: Solid State Commun. 22 (1977) 573.

77O Oudet, X.: see [77B1], p. 525.

77P Perkins, P.G.: Boron and Refractory Borides (Matkovich, V.I., ed.) Springer, Berlin, Heidelberg, New York 1977, p. 52.
78B Berrada, H., Mercuno, J. P., Etourneau, J., Hagenmuller, P., Shroff, A. M.: J. Less-Common Met. 59 (1978) 7.
78F Fujita, F. E.: J. Phys. Colloq. C 2, 40 (1979) 120.
78K Kasaya, M., Tarascon, J.M., Etourneau, J., Hagenmuller, P.: Mater. Res. Bull. 13 (1978) 751.
79C Cannon, J.F., Cannon, D.M., Hall, H.T.: in: High-Pressure Sci. Technol., 6th AIRAPT Conf., 1977, K.I. Timmermhaus, M.S. Barber ed., Plenum Press: New York, 1979, p. 1000.
79C1 Coey, J. M. D., Massenet, O., Kasaya, M., Etourneau, J.: J. Phys. Coloq. C 2,40 (1979) 333.
79F Fisk, Z., Johnston, D.C., Cornut, B., v. Molnar, S., Oserov, S., Calvo, R.: J. Appl. Phys. 50 (1979) 1911.
79G Gilchrist, K.E., Preston, S.D.: High Temp. High Press. 11 (1979) 643.
79K Kuzenkova, M.A., Kisly, P.S., Grabchuk, B.L., Bodnaruk, N.I.: J. Less-Common Met. 67 (1979) 217.
79K1 Kunii, S., Kasuya, T.: J. Phys. Soc. Jpn. 46 (1979) 13.
79M Moiseenko, L.L., Odintsov, V.V., Grushko, Yu.S.: Inorg. Mater. 15 (1979) 542.
79M1 Mercuno, J. P., Angelov, S., Etourneau, J.: J. Less-Common Met. 67 (1979) 237.
79O Oseroff, S., Calvo, R., Stankiewicz, J., Fisk, Z., Johnston, D. C.: Phys. Status Solidi (b) 94 (1979) K 133.
79S Swanson, L.W., Mc Neely, D.R.: Surf. Sci. 83 (1979) 11.
79V Vlasova, M.V., Kakazei, N.G., Kosolapova, T.Ya., Makarenko, G.N.: Sov. Phys. Semicond. 13 (1979) 107.
79V1 Volkonskaya, T. I., Kizhaev, S. A., Smirnov, I. A., Korsukova, M. M., Gurin, V. N.: Sov. Phys. Solid State 21 (1979) 375.
79W Werheit, H.: J. Less-Common Met. 67 (1979) 143.
80F Fujita, T., Suzuki, M., Isikawa, Y.: Solid State Commun. 33 (1980) 947.
80G1 Guy, C.N., v. Molnar, S., Etourneau, J., Fisk, Z.: Solid State Commun. 33 (1980) 1055.
80G2 Gurin, V.N., Korsukova, M.M., Karin, M.G., Sidorin, K.K., Smirnov, I.A., Shelikh, A.I.: Sov. Phys. Solid State 22 (1980) 418.
80H1 Holtzberg, F., v. Molnar, S., Coly, J.M.D.: Handbook on Semicond.., Vol. 3 (ed. Keller, S.P.) North Holland: Amsterdam, 1980, p. 803.
80H2 Higashi, I.: J. Solid State Chem. 32 (1980) 201.
80K Kasuya, T., Takegahara, K., Kasaya, M., Isikawa, Y., Fujita, T.: J. Phys. (France) Colloq. 41, C5 (1980) 161.
80L Lannin, J.S., Messier, R.: Phys. Rev. Lett. 45 (1980) 1119.
80T Tarascon, J. M., Etournean, J., Dordor, P., Hagenmuller, P., Kasaya, M., Coey, J. M. D.: J. Appl. Phys. 51 (1980) 574.
80W Weill, G., Smirnov, I.A., Gurin, V.N.: J. Phys. (France) Colloq. 41, C5 (1980) 185.
81K Ku, H.C., Meisner, G.P.: J. Less-Common Met. 78 (1981) 99.
81S Spear, K.E., Blanks, J.H., Wang, M.S.: J. Less-Common Met. 82 (1981) 237.
81T Tsagareishvili, G.V., Baimarashvili, I.A., Oganezov, K.A., Tabudsidze, M.L., Tsagareishvili, O.A.: J. Less-Common Met. 82 (1981) 131.
81T1 Tarascon, J.M., Etourneau, J., Dance, J.M., Hagenmuller, P., Georges, R., Angelov, S., v. Molnar, S.: J. Less-Common Met. 82 (1981) 277 (Proc. 7th Int. Symp. Boron, Borides and Rel. Compounds, Uppsala, Sweden, 1981).
82A Aita, O., Watanabe, T., Fujimoto, Y., Tsutsumi, K.: J. Phys. Soc. Jpn. 51 (1982) 483.
82L Lundström, T., Lönnberg, B., Törmä, B.: Phys. Scr. 26 (1982) 414.
82O Okusawa, M., Ichikawa, K., Matsumoto, T., Tsutsumi, K.: J. Phys. Soc. Jpn. 51 (1982) 1921.
82T Tsutsumi, K., Aita, O., Watanabe, T.: Phys. Rev. 25B (1982) 5415.
83P Paderno, Yu.B., Lundström, T.: Acta Chem. Scand. A 37 (1983) 609.
84L Lundström, T., Lönnberg, B., Westman, I.: J. Less-Common Met. 96 (1984) 229.
86K Kuz'ma, Yu.B., Mykhalenko, S.I., Akselrud, L.G.: J. Less-Common Met. 117 (1986) 29 (Proc. 8th Int. Symp. Boron, Borides, Carbides, Nitrides and Rel. Compounds, Tbilisi, Oct. 8 - 12, 1984).
87K Kuz'ma, Yu.B., Gurin, V.N., Korsukova, M.M., Aksel'rud, L.G.: Neorg. Mater. 23 (1987) 566.
90G Gridneva, I.B., Lazorenko, V.I., Lozko, D.V., Mil'man, Yu.B., Paderno, Yu.B., Tshugunova, S.I.: Poroshk. Metall. 12 (1990) 30.
91S Stein, H., Aselage, T.L., Emin, D.: in: Boron-Rich Solids, Proc. 10th Int. Symp. Boron, Borides and Rel. Compounds, Albuquerque, NM 1990 (AIP Conf. Proc. 231), D. Emin, T.L. Aselage, A.C. Switendick, B. Morosin, C.L. Beckel ed., American Institute of Physics: New York, 1991, p. 322.
95B Bat'ko, I., Bat'kova, M., Flachbart, K., Filippov, V.B., Paderno, Yu.B., Shicevalova, N.Yu., Wagner, Th.: J. Alloys Compounds 217 (1995) L1.
96G Gusev, A.I.: Russ. Chem. Rev. 65 (1996) 379.

97S Simeone, D., Deschanels, X., Berthier, B., Tessier, C.: J. Nucl. Mater. 245 (1997) 27.
98A Aselage, T.L.: J. Mater. Res. 13 (1998) 1786.
98S Shalamberidze, S., Kervalishvili, P., Kalandadze, G., Eristavi, A., Mickadze, V.: J. Mater. Process. Manufact. Sci. 6 (1998) 321 (Proc. NATO ASI on Material Science of Carbides, Nitrides and Borides, St. Petersburg, Russia, Aug. 12-22, 1998).
99A Ajmal, M., Khan, M.S., Shamin, A.: J. Solid State Chem. (2000) (Proc. 13th Int. Symp. Boron, Borides and Rel. Compounds, Dinard, France, Sept. 1999).
99S Schwetz, K.: (personal communication).
99W Werheit, H., Au, T., Schmechel, R., Paderno, Yu.B., Konovalova, E.S.: J. Solid State Chem. (2000) (Proc. 13th Int. Symp. Boron, Borides and Rel. Compounds, Dinard, France, Sept. 1999).
99Z Zaoui, A., Certier, M., Ferhat, M., Paés, O., Aourag, H.: Phys. Status Solidi (b) 212 (1999) 307.

Fig. 1.

$EuB_{6-x}C_x$. Lattice parameter vs. composition [78K].

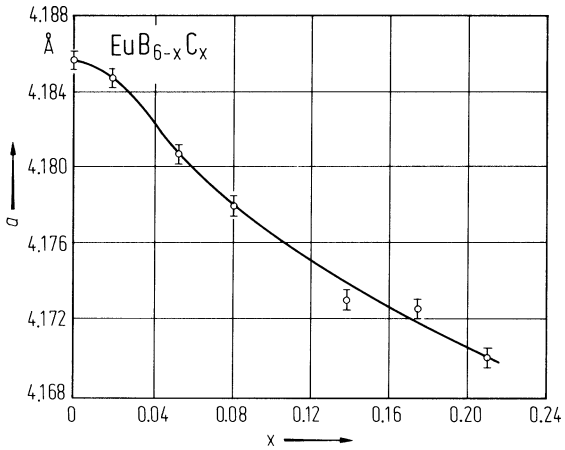

Fig. 2.

EuB_6. Energy diagram according to [77E, 73G].

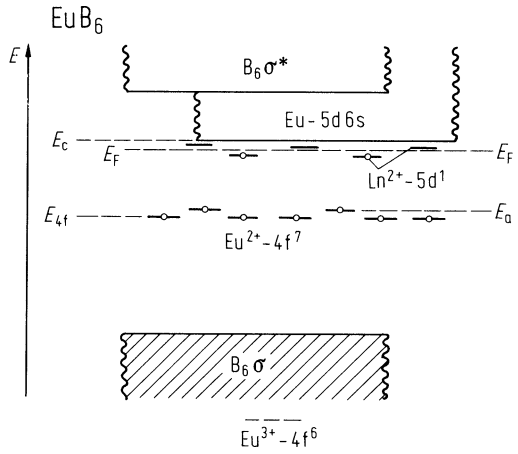

Fig. 3.

EuB_6. Self-consistent APW energy band structure for EuB_6 with the local-spin-density approximation exchange. **(a)** Majority spin electrons, **(b)** minority spin electrons [80H2].

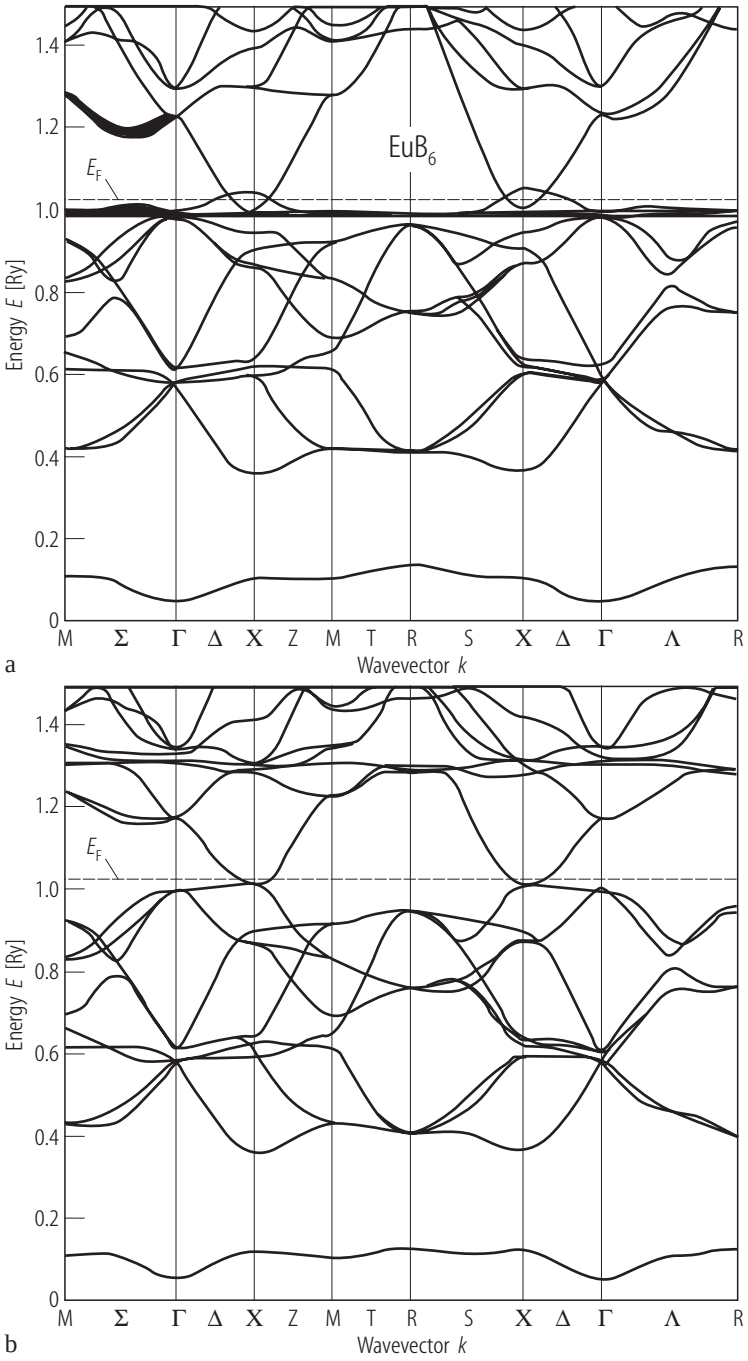

Fig. 4.

EuB_6. Partial density of states for various bands as a function of energy near E_F. The number N shows that the density of states is due to the N-th band. For the 17th and the 18th bands of the majority spin electrons (also for the 10th and 11th bands of the minority spin electrons), the energies of the two bands were exchanged near the X points, so that the bands cross each other around the X point [80H2].

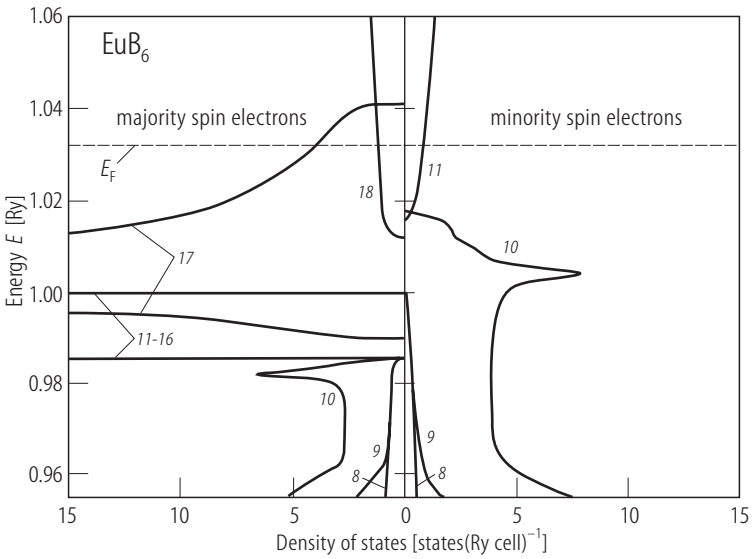

Fig. 5.

EuB_6. FIR absorption spectrum calculated from the reflectivity spectrum using a Kramers-Kronig transformation. Empirical slope for the free carrier absorption ($\propto \lambda^2$ for phonon scattering) subtracted from the measured absorption approximately yields the interband absorption (lower curve).[99W].

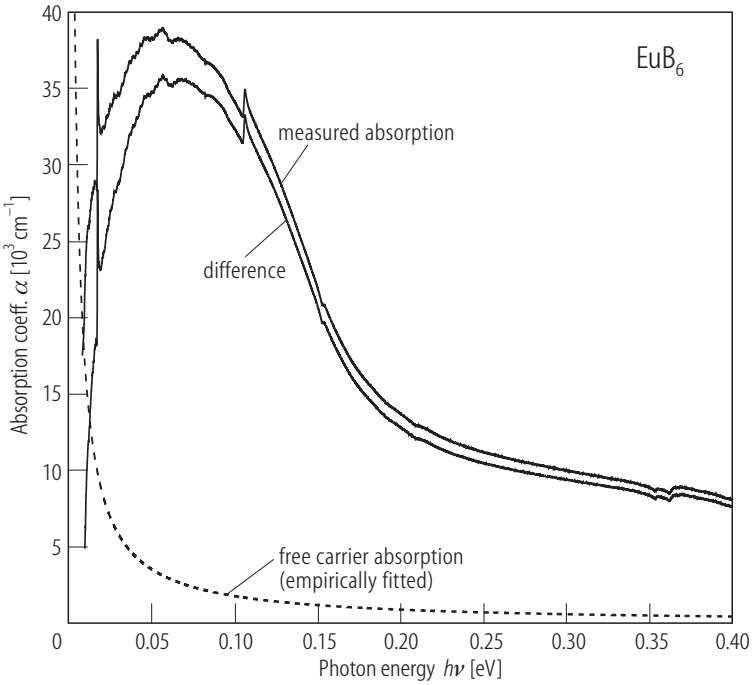

Fig. 6

EuB_6. a) ESR line width vs. temperature at 35.47 GHz. b) Temperature dependence of the ESR resonance points at 35.47 GHz [79K]. $\Delta H_{p\text{-}p}$: peak to peak line width; H_z: resonance field in z-direction. (For qualitatively similar results at 24.58 GHz, see original paper.).

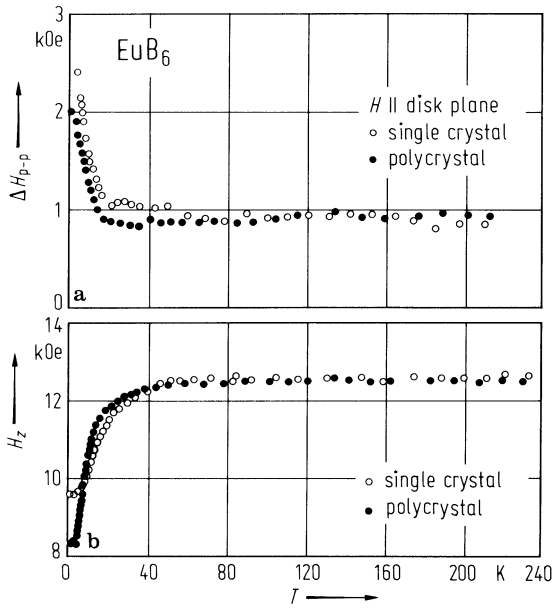

Fig. 7.

EuB_6. Absorption coefficient α vs. photon energy. Insert: Plot in relative units according to direct forbidden interband transitions [80G2].

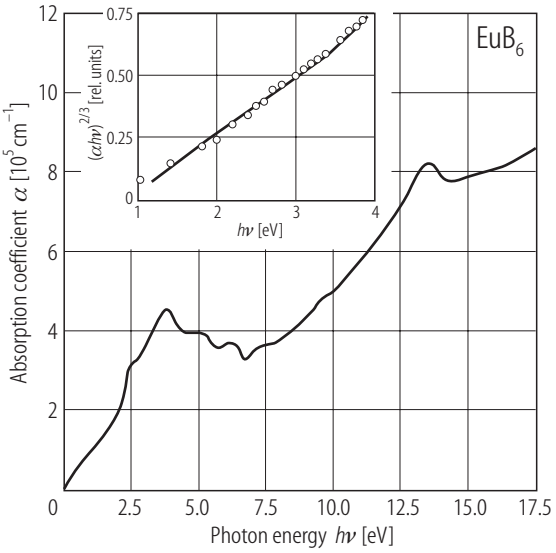

Fig. 8.

$EuB_{6-x}C_x$. Paramagnetic Curie temperature vs. composition [78K, 79K].

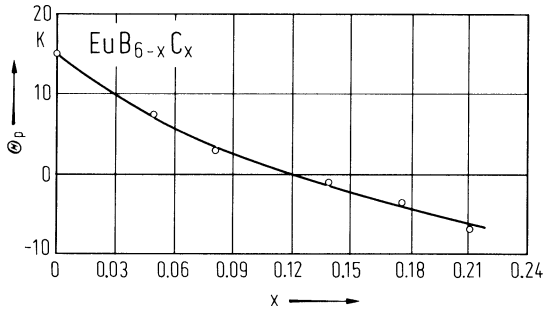

Fig. 9.

$EuB_{6-x}C_x$. Electrical resistivity for x = 0 and x = 0.05 vs. temperature [78K, 79K].

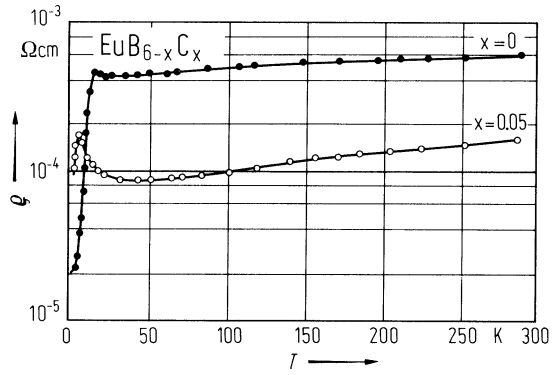

Fig. 10.

EuB_6 :C. Lattice parameter depending on the carbon content; full circles, [79S], open circles, [78K]. Preparation of the samples in [79S] by hotpressing at 1400°C and subsequent annealing at the temperatures marked in the diagram to determine the temperature-dependent solubility limits.

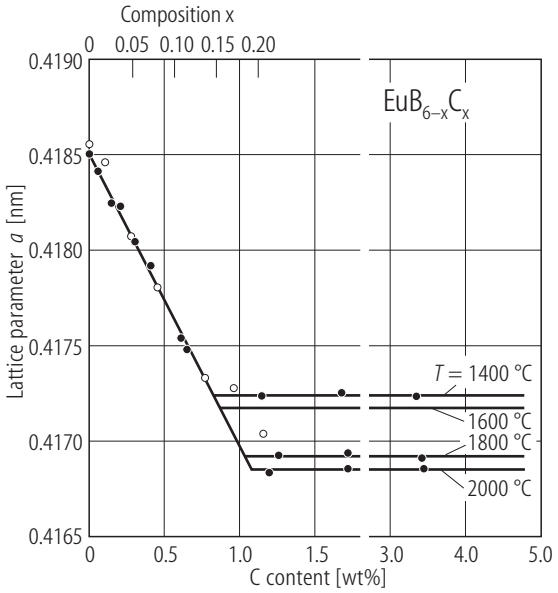

Fig. 11.

EuB_6:C, YbB_6:C. EuB_6: Carrier concentration vs. C content; data at C =0.43 at. % and 0.71 at. % from [81T]. The points for the pure crystals suggest that the upper limit of 0.1 at.% C, given for the purest samples, is too high and the real C content is about 0.05 at. % only. The arrow marks the relation between the chemically determined total C content of 1.1 at.% and that one in the EuB_6 lattice, which according to experience is roughly estimated to be about 25 % lower in sintered EuB_6 [99S]. YbB_6: Only the data for 0.43 at. % C [81T] and upper carbon limit for the pure crystal are available. A dependence similar to that of EuB_6 is assumed [99W].

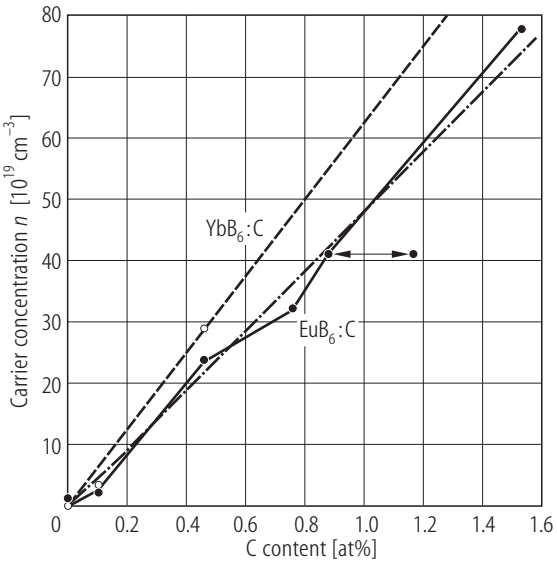

Fig. 12.

EuB_6. Variation of the paramagnetic Curie temperature Θ vs. x for $EuB_{6-x}C_x$ [81T].

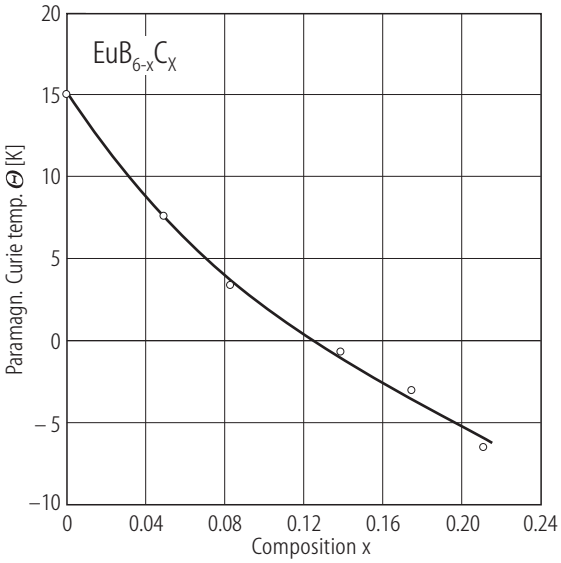

Fig. 13.

EuB_6. FT Raman spectrum of $EuB_{5.9}C_{0.1}$ at 300 K; Raman intensity vs. Raman shift. The reproducible Raman peaks are indicated by arrows [97S].

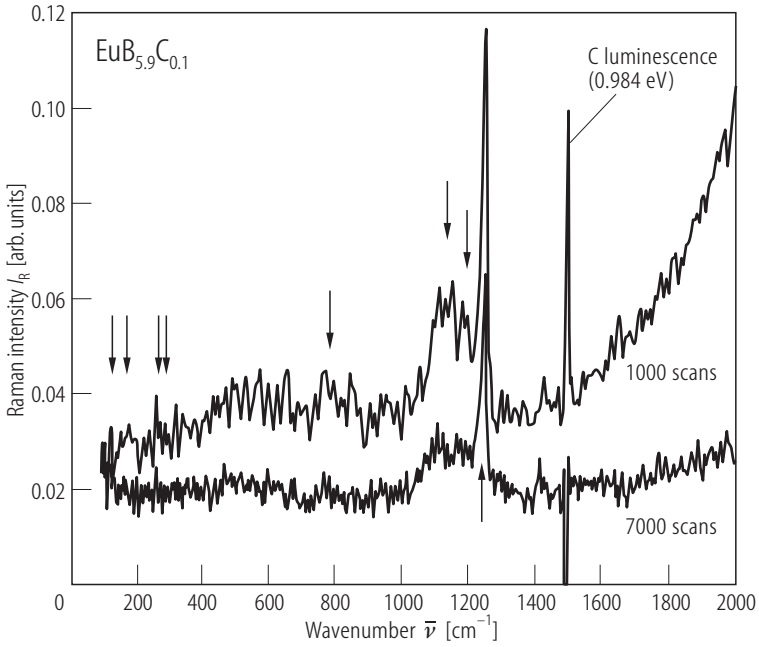

Fig. 14.

Metal-hexaborides (metallic). IR reflectivity spectra of single-crystal pure YB_6, LaB_6, CeB_6, SmB_6, $Sm_{0.8}B_6$ and TbB_6.. Some of the spectra are vertically shifted to avoid superposition. The amount of the shift is indicated at the spectra in the diagram. It is assumed that the phonon spectra occur in the spectra because symmetry selection rules are lifted in consequence of structural distortions [99W].

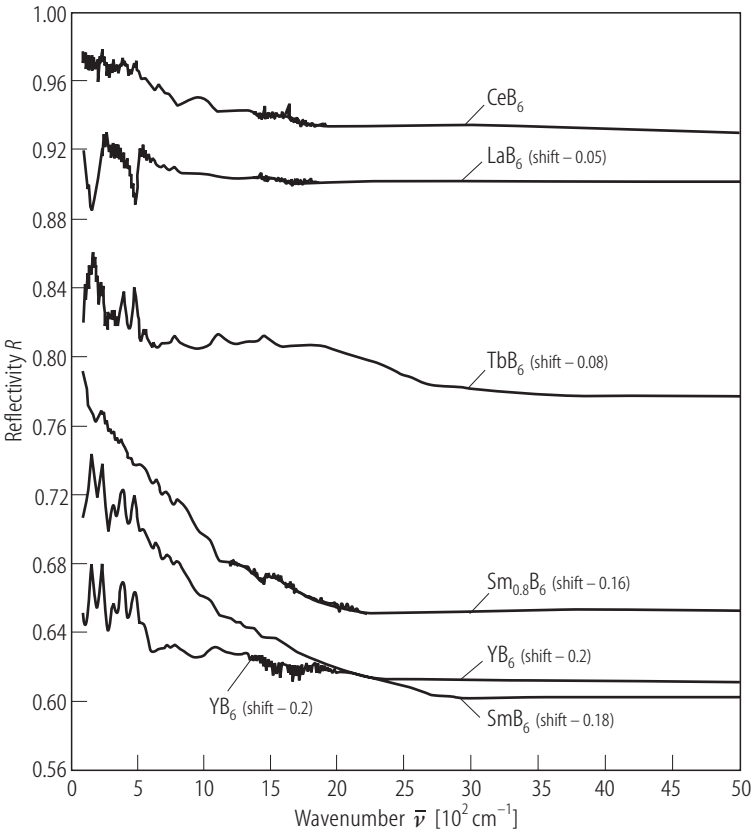

Fig. 15.

Metal hexaborides. Pressure dependence of the electrical resistivity; $\rho(p)/\rho(0)$ vs. hydrostatic pressure p. Full lines, monocrystalline LaB_6, EuB_6 and YbB_6 [91S10], dashed lines, LaB_6, SmB_6 prepared from starting ratios Sm:B 1/7, 1/9, 1/12 (effect increases this way), YbB_6, EuB_6 [81K].

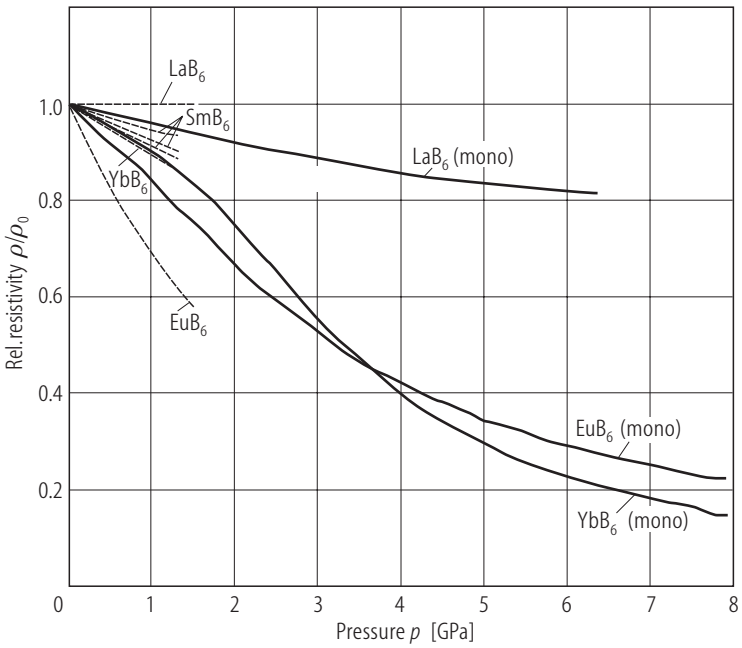

Fig. 16.

EuB_6. Resistivity of a single crystal at $B = 0$ and $B = 1.5$ T vs. temperature [80G1]. Insert: same plot at $B = 0$ and $B = 0.95$ T. $\Delta\rho/\rho$ changes sign at about 5.5 K [79W] (cp. also [77I]).

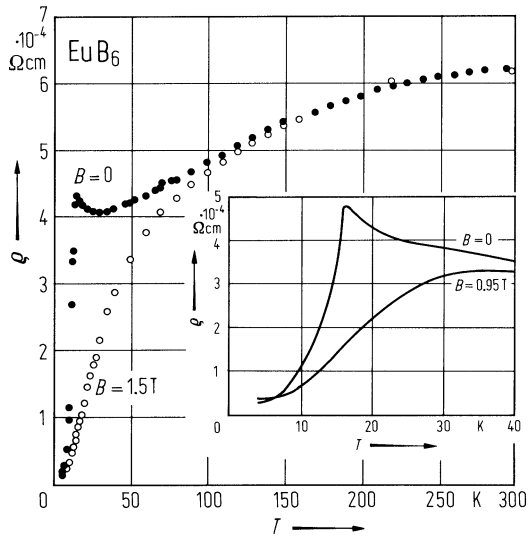

Fig. 17.

EuB_6, YbB_6. Electrical conductivity vs. reciprocal temperature [77E, 73M, 73B]. Cp. also [69F, 75S].

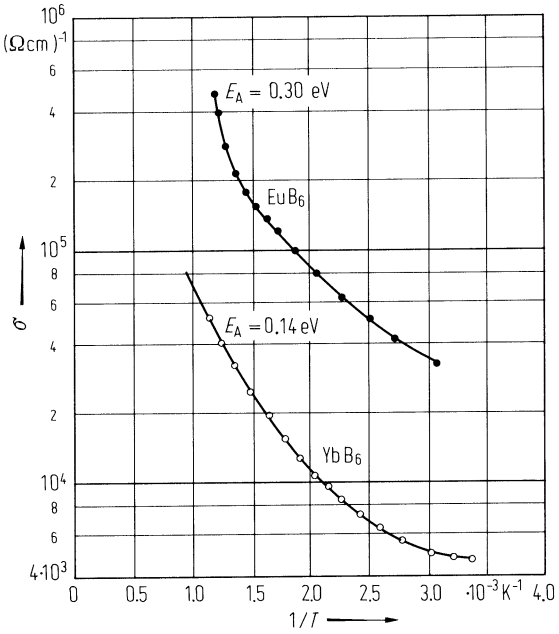

Fig. 18.

$La_xEu_{1-x}B_6$. Resistivity vs. temperature [77E, 74M1].

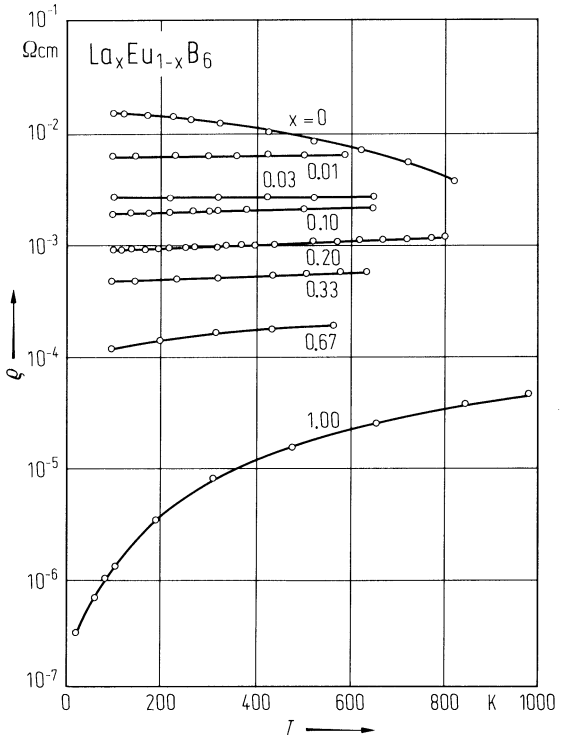

Fig. 19.

EuB_6. Magnetoresistance vs. magnetic field (squared) at 77 K for different pressures [79W].

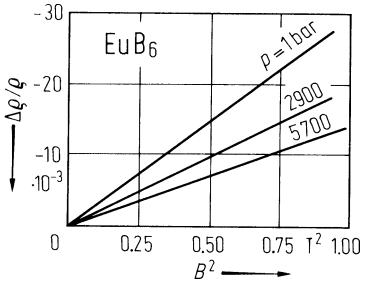

Fig. 20.

EuB_6. Temperature dependence of the electrical resistivity of single-crystalline EuB_6. Insert: Low-temperature resistivity in the range of the magnetic transition; circles, experimental data; solid line, calculated fit to the data below 10 K [98S].

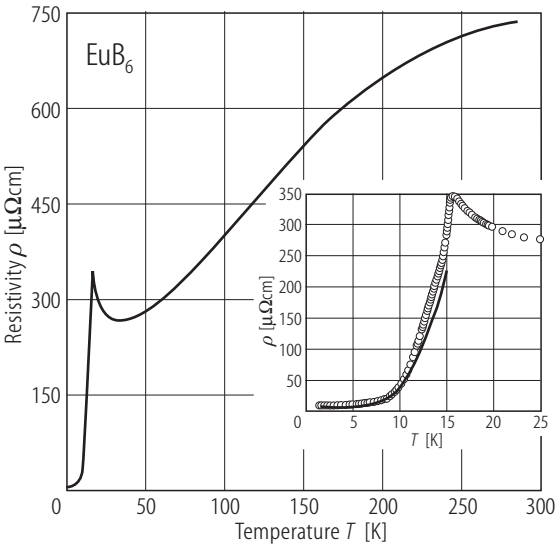

Fig. 21.

EuB_6. Magnetoresistance measured for B || [100] at 15 K [98S].

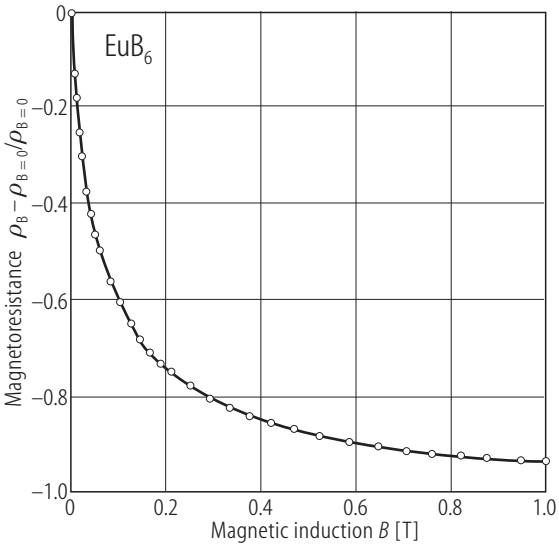

Fig. 22.

EuB_6. a) Hall resistivity $e_H = R_H \cdot B + R_s \cdot 4\pi M$ (R_H = normal Hall coefficient, R_s = anomalous Hall coefficient, B = magnetic induction, M = magnetization of the sample) at 4.2 K vs. magnetic induction [80G1]. Solid curve calculated with $R_H = -3.7 \cdot 10^{-2}$ cm^3 C^{-1} and $R_s = -4.8 \cdot 10^{-3}$ cm^3 C^{-1}. b) Relative Hall resistivity in the paramagnetic region $e_H/H_A = R_H + \{(1-N)R_H + R_s\} \cdot 4\pi\chi_{eff}$ (H_A = applied field; N = 0.633 (demagnetizing factor)) vs. the effective susceptibility $\chi_{eff} = \chi/(1 + 4\pi N\chi)$ [80G1].

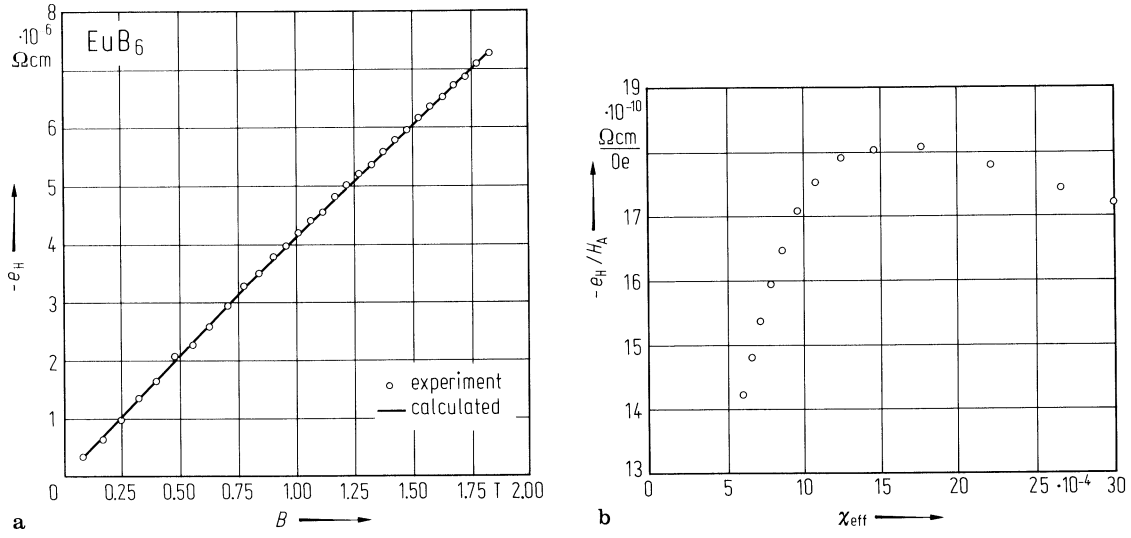

Fig. 23.

EuB_6. Electrical resistivity ratios $\rho(p)/\rho(0)$ vs. hydrostatic pressure [79G]. Curve I: EuB_6 prepared with a stoichiometric ratio Eu to B in the starting charge; curves II and III: with B surplus.

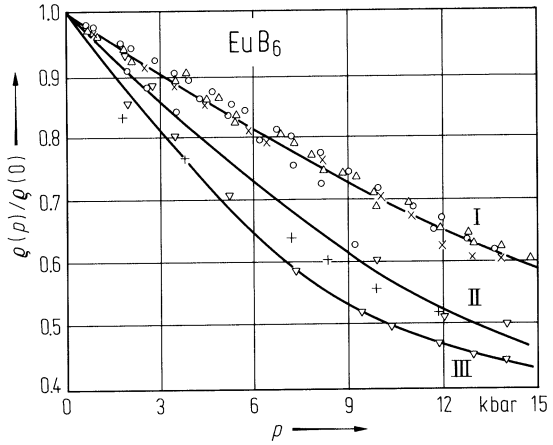

Fig. 24.

EuB_6. Magnetoresistance vs. magnetic field (squared) at 77 K for different pressures [79W].

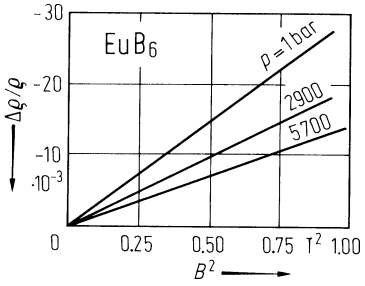

Fig. 25.

EuB_6, YbB_6. Thermoelectric power vs. temperature [77E, 73M, 73B]. Cp. also [75S].

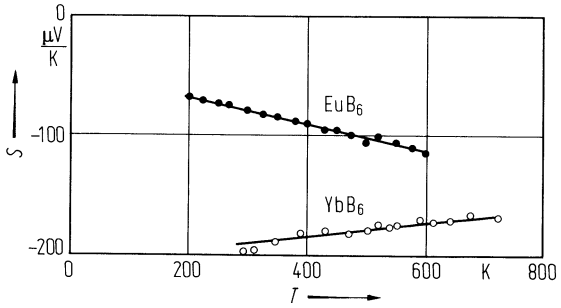

Fig. 26

Metal hexaborides. Pressure dependence of the thermoelectric power S for LaB_6, YbB_6 and EuB_6 [81K].

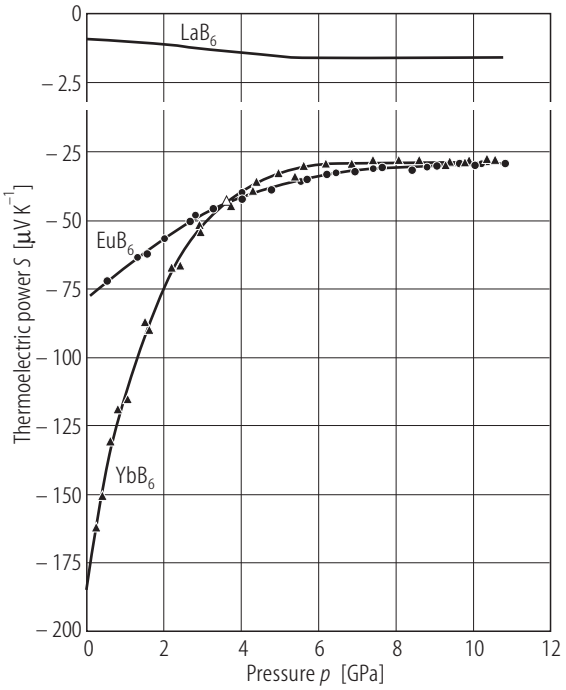

Fig. 27.

EuB_6 :C. Real part of the dielectric function vs. wavenumber squared. The extrapolation to $\varepsilon_1 = 0$ yields the plasma frequencies, the extrapolation to wavenumber = 0 yields the lattice dielectric constant [99W].

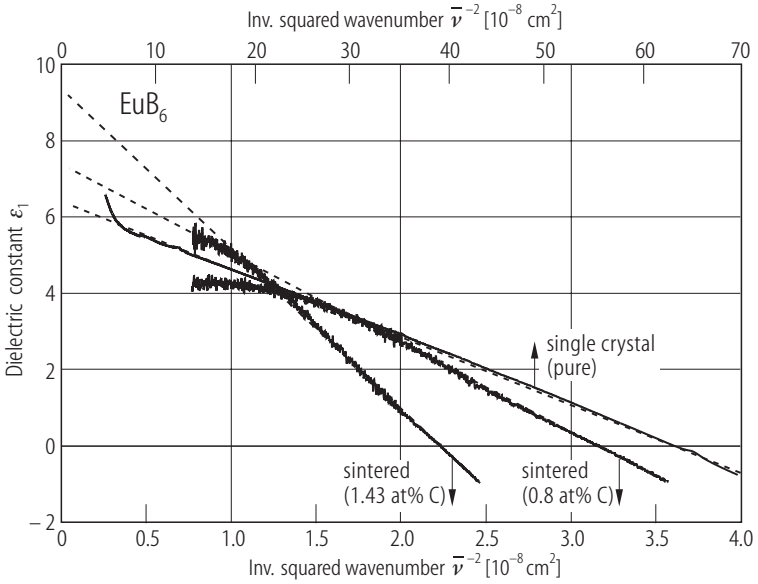

Fig. 28.

EuB_6. Dielectric function vs. photon energy. ε_1, real part, ε_2 imaginary part, $-\mathrm{Im}\,\varepsilon^{-1}$ energy loss function [81S].

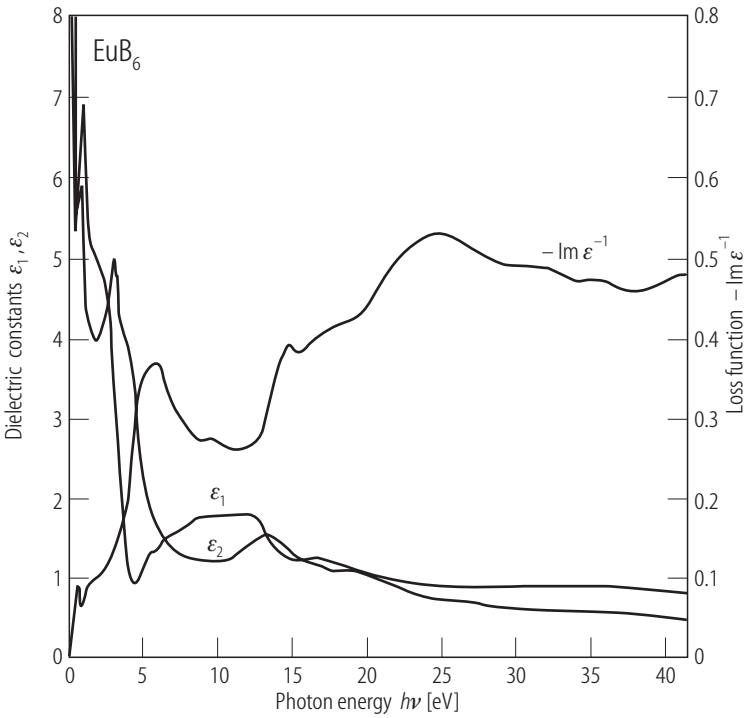

Fig. 29.

Metal hexaborides. Optical reflectivity spectra; R vs. photon energy. Long-dashed curve, LaB_6, solid curve, SmB_6, short-dashed curve, EuB_6 [81S].

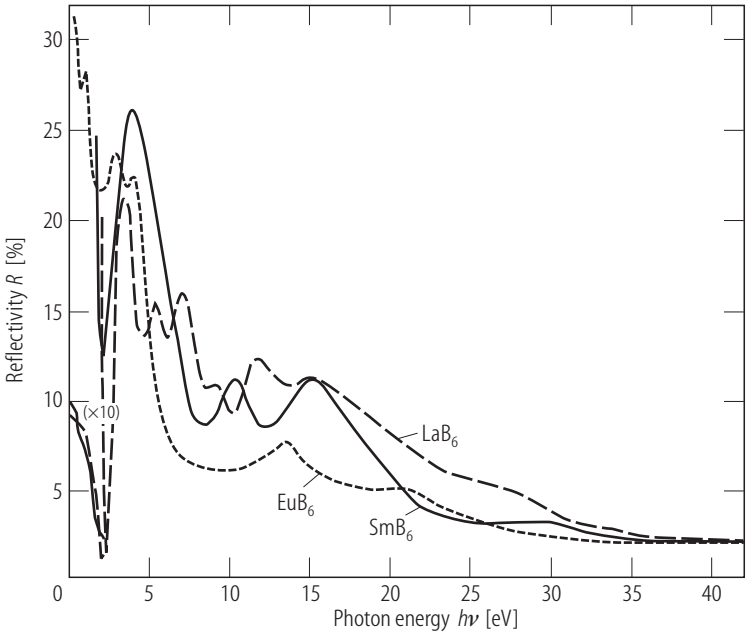

Fig. 30.

EuB_6. Reflectivity vs. wavenumber (pure EuB_6, ~0.8 at.% C content, 1.43 at.% C content), insert: plasmon-phonon-polariton resonances; for resonance frequencies see lattice properties [99W].

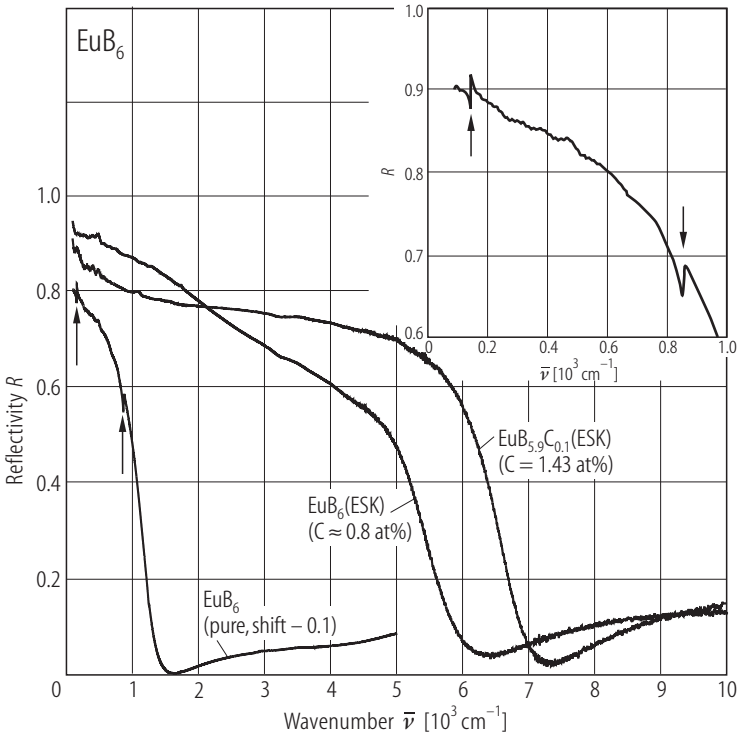

Fig. 31.

EuB_6. a) Heat capacity vs. temperature. Open circles: ferromagnetic samples; open triangles: antiferromagnetic samples, full circles: LaB_6 for comparison [80F]. b) Low temperature heat capacity of antiferromagnetic EuB_6 in different fields applied along a [100] axis: a: $H = 0$, b: $H = 0.2$ T, c: $H = 0.6$ T, *d*: $H = 1.2$ T. Data for the ferromagnetic EuB_6 at $H = 0$ are also shown by the dashed curve [80F].

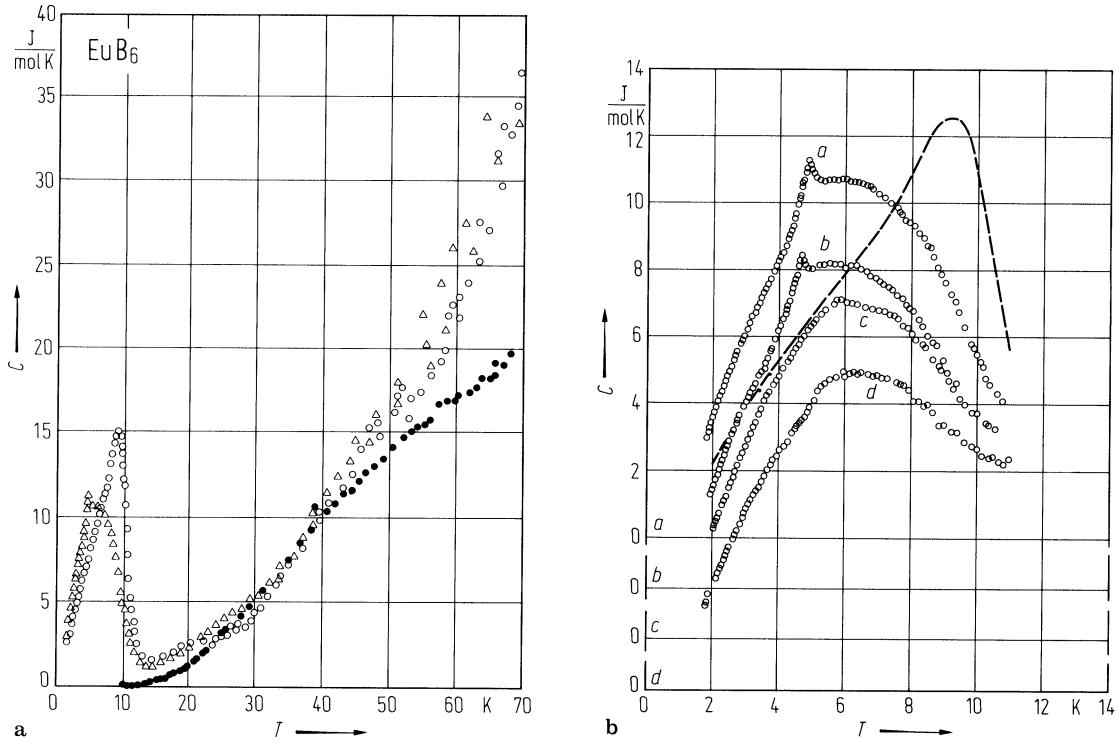

Fig. 32.

Metal hexaborides. Entropy vs. T for LaB_6, ferromagnetic EuB_6, antiferromagnetic EuB_6 [80F].

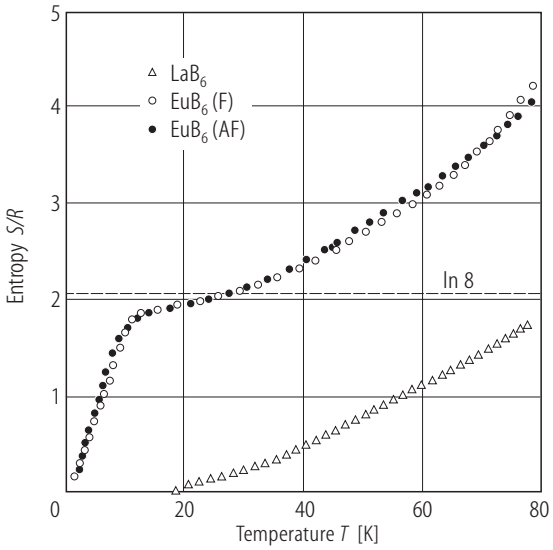

Fig. 33.

EuB_6. Field dependence of the heat capacity measured on a crystal showing no anomaly at T_{c1}; solid line, calculated [98S].

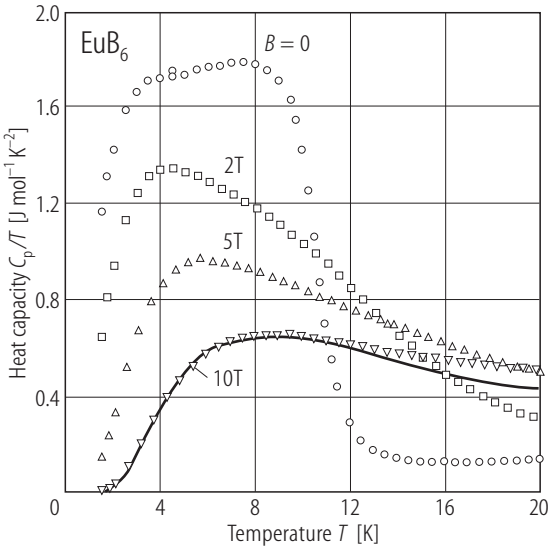

Fig. 34.

EuB_6. Magnetic susceptibility. **(a)** Inverse susceptibility $1/\chi_m$ vs. T; B = 0.1 T, in different directions. **(b)** χ_m vs. T for B || [100]; solid line, 0.005 T, circles, 0.01T; squares, 0.02T; up triangles, 0.05T; down triangles, 0.1T; diamonds, 0.2T **(c)** χ_m for B || [111]; for symbols see **(b)** (for B || [110] see [98S]).

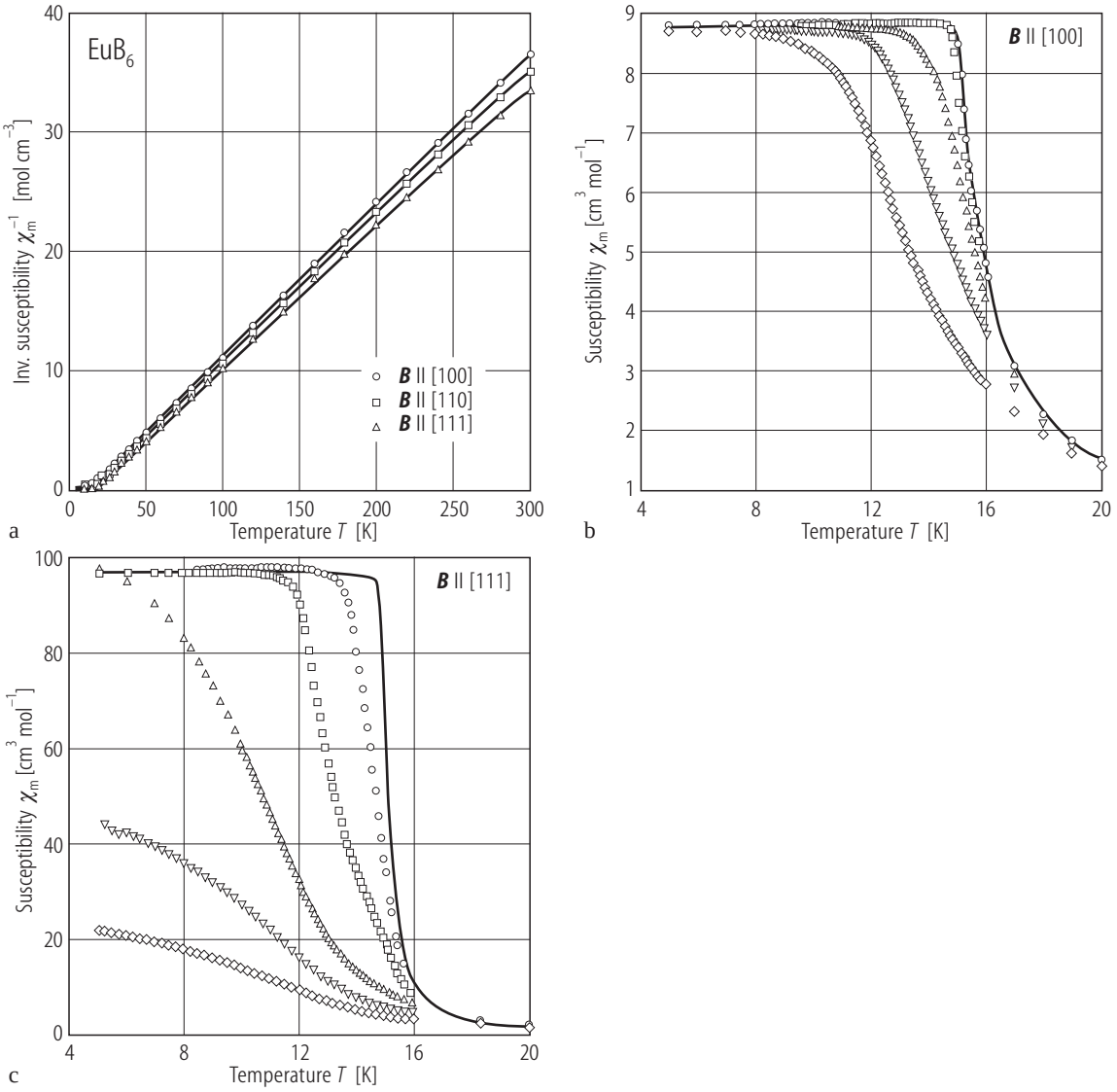

Fig. 35.

EuB_6. Exchange field in bulk (I) and low-electron-density (II) material vs. temperature. Results obtained by EPR [76G1].

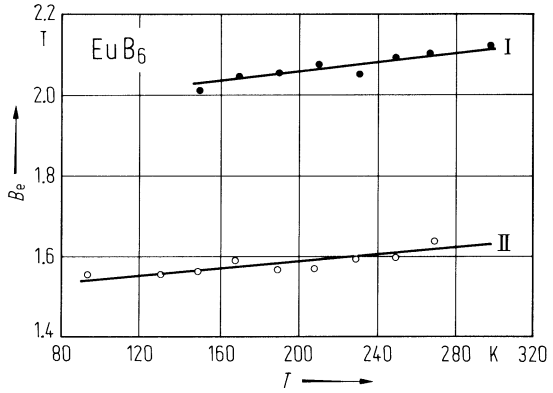

Fig. 36.

EuB_6. Magnetic phase diagram derived from Mössbauer (full circles) and magnetic (triangles) data. Ordering temperatures vs. lattice parameter (P: paramgnetic; F: ferromagnetic; M: micromagnetic; AF: antiferromagnetic). The second scale relates *a* to the approximate conduction electron concentration. (Open circles: paramagnetic Curie temperatures according to [78K]). [79C1]. See also [80G1, 80T].

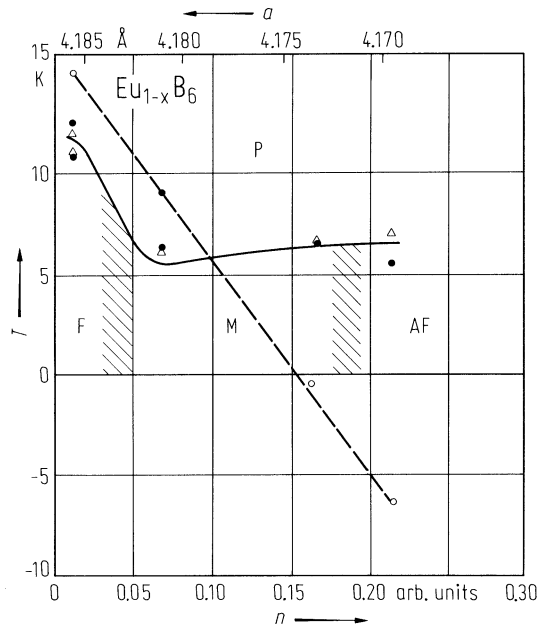

Fig. 37.

$Eu_{1-x}B_6$. Low field magnetic susceptibility of an Al–grown $Eu_{1-x}B_6$ single crystal vs. temperature (the units of χ assume an exact EuB_6 composition) Insert: Saturation magnetic moment per Eu ion, p_A, vs. temperature derived from Arrot plots (accuracy 20%) [79F].